International Journal of Nanomedicine

Dovepress
open access to scientific and medical research

Open Access Full Text Article

ORIGINAL RESEARCH

Chitosan nanofiber scaffold improves bone healing via stimulating trabecular bone production due to upregulation of the Runx2/osteocalcin/alkaline phosphatase signaling pathway

This article was published in the following Dove Press journal:
International Journal of Nanomedicine
22 September 2015
Number of times this article has been viewed

Ming-Hua Ho[1,2]
Chih-Jung Yao[3]
Mei-Hsiu Liao[4]
Pei-I Lin[4]
Shing-Hwa Liu[5]
Ruei-Ming Chen[2,4,6]

[1]Department of Chemical Engineering, National Taiwan University of Science and Technology, [2]Cell Physiology and Molecular Image Research Center, Taipei Medical University-Wan Fang Hospital, [3]Department of Internal Medicine, School of Medicine, [4]Graduate Institute of Medical Sciences, College of Medicine, Taipei Medical University, [5]Institute of Toxicology, College of Medicine, National Taiwan University, [6]Anesthetics and Toxicology Research Center, Taipei Medical University Hospital, Taipei, Taiwan

Abstract: Osteoblasts play critical roles in bone formation. Our previous study showed that chitosan nanofibers can stimulate osteoblast proliferation and maturation. This translational study used an animal model of bone defects to evaluate the effects of chitosan nanofiber scaffolds on bone healing and the possible mechanisms. In this study, we produced uniform chitosan nanofibers with fiber diameters of approximately 200 nm. A bone defect was surgically created in the proximal femurs of male C57LB/6 mice, and then the left femur was implanted with chitosan nanofiber scaffolds for 21 days and compared with the right femur, which served as a control. Histological analyses revealed that implantation of chitosan nanofiber scaffolds did not lead to hepatotoxicity or nephrotoxicity. Instead, imaging analyses by X-ray transmission and microcomputed tomography showed that implantation of chitosan nanofiber scaffolds improved bone healing compared with the control group. In parallel, microcomputed tomography and bone histomorphometric assays further demonstrated augmentation of the production of new trabecular bone in the chitosan nanofiber-treated group. Furthermore, implantation of chitosan nanofiber scaffolds led to a significant increase in the trabecular bone thickness but a reduction in the trabecular parameter factor. As to the mechanisms, analysis by confocal microscopy showed that implantation of chitosan nanofiber scaffolds increased levels of Runt-related transcription factor 2 (Runx2), a key transcription factor that regulates osteogenesis, in the bone defect sites. Successively, amounts of alkaline phosphatase and osteocalcin, two typical biomarkers that can simulate bone maturation, were augmented following implantation of chitosan nanofiber scaffolds. Taken together, this translational study showed a beneficial effect of chitosan nanofiber scaffolds on bone healing through stimulating trabecular bone production due to upregulation of Runx2-mediated alkaline phosphatase and osteocalcin gene expressions. Our results suggest the potential of chitosan nanofiber scaffolds for therapy of bone diseases, including bone defects and bone fractures.

Keywords: chitosan nanofibers, bone healing, micro-computed tomography, bone histomorphometry, Runx2/OCN/ALP

Introduction

A bone's structure is dynamically maintained by bone remodeling, a process balanced by osteoblast-mediated bone formation and osteoclast-mediated bone resorption.[1,2] Imbalances of bone remodeling usually suppress bone healing or lead to bone diseases such as osteoporosis and bone defects.[3] Bone fractures are accidents that often occur in modern people. In addition, osteoporosis-related bone fractures are a major risk of inducing disability and even death.[4] After a fracture occurs, bone healing can

Correspondence: Ruei-Ming Chen
Graduate Institute of Medical Sciences, College of Medicine, Taipei Medical University, 250 Wu-Xing Street, Taipei 110, Taiwan
Tel +886 2 2736 1661 ext 3222
Fax +886 2 8662 1119
Email rmchen@tmu.edu.tw

spontaneously take place in order to reestablish the original physical and mechanical properties of the tissue.[5] Fracture healing comprises three separate stages: the early inflammatory stage, the repair stage, and the late remodeling stage. During bone healing, many systemic and local factors are involved.[4,6] Osteogenesis, a continuous progression of osteoprogenitor proliferation, matrix maturation, and osteoblast maturation, is one such factor and plays a crucial role in stimulating fracture healing.[7,8] Nevertheless, there is so far no effective drug developed for therapy of bone fractures. Thus, discovering proper biomaterials that can promote osteogenesis would be beneficial to establish alternative strategies for therapy of bone fractures and defects.

Chitosan was shown to promote bone remodeling, so it is generally used as scaffold matrices for management of bone trauma and tumors.[9] Chitosan is widely used for cartilage tissue engineering, wound healing, and orthopedic applications because of its high biocompatibility, biodegradability, porous structure, and intrinsic antibacterial nature.[10–12] However, because chitosan scaffolds alone are not osteoconductive, the composite materials with chitosan are developed to imitate bone properties.[13] The composites of chitosan with hydroxyapatite or calcium phosphate have been shown to improve bone healing.[14,15] In comparison, electrospun products of chitosan possess higher surface areas and porosity.[16] Previous studies showed that chitosan nanofiber scaffolds can be applied as a biomimetic extracellular matrix (ECM) to stimulate regeneration of neurons or proliferation of endothelia and smooth muscle cells.[17,18] Furthermore, chitosan nanofibers can expand the resistance of porous scaffolds to compressive loading stress and thus provide greater structural protection to mesenchymal stem cells.[19,20] Shin et al reported the biocompatibility of the chitosan nanofiber membrane and its biological effects on bone regeneration.[21] In our laboratory, we have developed chitosan nanofibrous scaffolds and examined their beneficial effects on the proliferation and maturation of osteoblasts.[22] Accordingly, electrospun nanofibers of chitosan have better properties and wider applications than its free form in biomedicine.

A large array of molecular and cellular events is involved in regulating bone development and fracture healing.[23,24] These events are tightly linked by sequential expressions of osteoblast differentiation-related genes. Runt-related transcription factor 2 (Runx2) is implicated as an essential transcription factor for osteoblast differentiation and mineralization.[25,26] Wohl et al reported that Runx2 expression is associated with osteogenesis and bone repair.[27] Moreover, alkaline phosphatase (ALP) and osteocalcin (OCN) are two typical osteoblast biomarkers that participate in controlling osteoblast function and ECM mineralization in osteogenesis and bone remodeling.[28,29] Previous studies demonstrated that upregulation of ALP and OCN in osteoblasts is directly correlated with cell differentiation and maturation.[7,28] Takahashi et al further showed that Runx2 stimulated differentiation of multipotential mesenchymal ROB-C26 cells into mature osteoblasts by regulating OCN and ALP gene expressions.[30] Furthermore, our previous study demonstrated the roles of Runx2 in mediating nitric oxide-induced osteoblast protection against apoptotic insults through regulating antiapoptotic *bcl-2* gene expression.[31] Osteoblasts play a key role in bone formation.[2] Interestingly, when we seeded osteoblasts onto chitosan nanofiber scaffolds, Runx2 signaling events were activated, and the growth and maturation of osteoblasts concurrently improved.[22] To confirm our previous in vitro findings, this translational study was further aimed to investigate the effects of chitosan nanofiber scaffolds on bone healing using an animal model of bone defects and determine possible mechanisms from the viewpoint of Runx2-mediated regulation of ALP and OCN expressions.

Materials and methods

Materials

Chitosan with a molecular weight of 210 kDa, trifluoroacetic acid (TFA), and 3,3′-diaminobenzidine were purchased from Sigma-Aldrich (St Louis, MO, USA). Dichloromethane (DCM) was purchased from Tedia (Fairfield, OH, USA).

Preparation of chitosan nanofibers

Chitosan nanofibers were prepared according to our previous method.[22] To produce optimal chitosan nanofiber products, various ranges of chitosan concentrations, applied voltages, distances between the needle and collector, feed rates, solution temperatures, and chamber temperatures were first examined (Table 1). Finally, chitosan at 80 mg/mL was dissolved in TFA/DCM at a volume ratio of 7:3, and then

Table 1 Applicable ranges and optimized values of operational parameters for preparing chitosan electrospinning nanofibers

Parameter	Range of values	Optimal condition
Chitosan concentration (mg/mL)	50–80	80
Applied voltage (kV)	10–20	17
Distance between the needle and collector (cm)	8–16	12
Feed rate (mL/h)	0.2–0.5	0.2
Solution temperature (°C)	20–32	32
Chamber temperature (°C)	24–37	32

the electrospinning mixtures were stirred for 24 hours into well-mixed homogeneous solutions. The tip-to-collector distance was 12 cm, and the applied voltage was 17 kV (Table 1). The electrospinning setup used in this study consisted of three major components: a power supply using direct current that could generate a voltage of up to 30 kV, a 3 mL syringe with a metallic needle of a 0.65 mm inner diameter that could control the flow rate of a scientific pump (model 780/00, KD Scientific, Holliston, MA, USA), and a collector made from aluminum foil for fiber collection (KD Scientific).

Scanning electron microscopy

The surface morphologies of chitosan nanofiber scaffolds were scanned and photographed using scanning electron microscopy as described previously.[22] At first, surfaces of the chitosan nanofibers were coated with gold. Then, samples were scanned at an accelerating voltage of 15 kV using scanning electron microscopy (JSM-6390LV; JEOL, Tokyo, Japan).

Animals

All procedures were performed according to the National Institutes of Health Guidelines for the Use of Laboratory Animals and were approved by the Institutional Animal Care and Use Committee of Taipei Medical University-Wan Fang Hospital (Taipei, Taiwan). Male C57LB/6 mice weighing 20–25 g were purchased from the Animal Center of the College of Medicine, National Taiwan University (Taipei, Taiwan). Before starting our experiments, mice were allowed to acclimatize for 1 week in animal quarters with air-conditioning and an automatically controlled photoperiod of 12 hours of light daily.

Bone defect model and implantation of chitosan nanofiber scaffolds

A metaphyseal bone defect in the proximal femur was produced following a method described previously.[32] Briefly, mice were anesthetized with propofol (100 mg/kg body weight). One hole in each proximal femur was then expanded into a round metaphyseal bone defect using a blunt 1.0 mm drill bit fixed to a finger handle. Defects in both proximal femurs were drilled through the anterolateral cortical bone into the metaphyseal cancellous bone to the opposite cortex (depth: ~2 mm; Figure 1). Chitosan nanofiber scaffolds were rinsed in phosphate-buffered saline (PBS) (0.14 M NaCl, 2.6 mM KCl, 8 mM Na_2HPO_4, and 1.5 mM KH_2PO_4), subsequently exposed to ultraviolet light for 30 minutes, and then implanted into the bone defect site of the left femur as the scaffold-treated group. The right femurs were subjected to the same procedure as done in the left ones, but the bone defect sites were not treated with chitosan nanofibers and served as the control group. The wounds were sutured with 4.0 Nylon and observed. Animals were allowed free unrestricted weight bearing after recovery from anesthesia. The body weights were measured after surgery. In this study, the mice (n=9) were sacrificed on day 21 after implantation of the chitosan nanofiber scaffolds.

Assessment of hepatotoxicity and nephrotoxicity

Toxicities of the chitosan nanofiber scaffolds to the liver and kidneys were assayed using histological analyses as described previously.[33] After implantation of chitosan nanofiber scaffolds for 21 days, the animals were sacrificed, and the

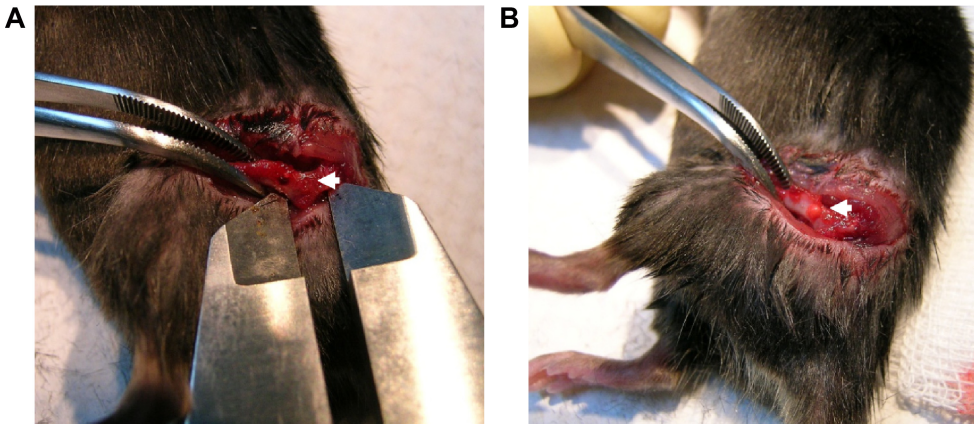

Figure 1 An animal model of bone defects.
Notes: Male C57LB/L mice were anesthetized, and a metaphyseal bone defect was drilled in the proximal femur (**A**). After rinsing in phosphate-buffered saline and subsequent exposure to ultraviolet light for 30 minutes, chitosan nanofiber scaffolds were implanted into the bone defect (**B**). The wound was sutured, and the animals were allowed free unrestricted weight-bearing after recovery from anesthesia. Only one defect was created in each proximal femur of an animal, and totally nine animals were treated in this study. Arrows indicate the bone defect sites.

liver and kidneys were collected. These tissue samples were fixed with 4% formaldehyde for 24 hours. After fixation, samples were embedded in paraffin. Xylene and gradient ethanol were used for deparaffinization. Tissue specimens were cut into 5 μm sections and stained with hematoxylin and eosin. Stained signals in specimens were observed and photographed using a light microscope (Nikon Corporation, Tokyo, Japan).

Microcomputed tomography

Bone healing was evaluated using microcomputed tomography (μCT) as described previously.[34] After implanting the chitosan nanofiber scaffolds into the bone defect sites for 21 days, the animals were sacrificed, and the femurs were collected. After removing the muscle and connective tissues, the femurs were weighed and photographed. X-ray transmission was conducted using a Skyscan 1076 μCT scanner (Skyscan, Antwerp, Belgium). Additionally, trabecular bone production was scanned and quantified using a μCT scanner (Skyscan). The scanning axis nominally coincided with the diaphyseal axis of the control femur. Femurs with a bone defect were scanned using the same parameters (9 μm per slice, 50 kV, 140 μA, 0.5 mm Al filter, 3,300 ms exposure time). High-resolution images of the femurs were generated into a 3D polygonal resampling using an Skyscan 3D-Creator software (Skyscan), and morphometric parameters were calculated for trabecular bone regions of interest (ROIs) using a Skyscan CT-Analyser (Skyscan). Moreover, trabecular bone was analyzed to determine numbers and thickness of trabecular bone. The trabecular pattern factor (TPF), a parameter of trabecular bone connections within an ROI, was estimated using the Skyscan CT analyzer software. A smaller value of the TPF means that trabecular bone was more connected.[35]

Bone histomorphometry

Bone repair was further assayed using histological analyses as described previously.[36] After implantation of chitosan nanofiber scaffolds for 21 days, the animals were sacrificed, and their femurs were collected. At first, these bone samples were cleaned to remove the muscle and the connective tissues. Then, the femurs were fixed in 4% formaldehyde, embedded in paraffin, and cut transversally into 5 μm sections. Xylene and gradient ethanol were used for deparaffinization. The specimen slices were stained with hematoxylin and eosin. Stained images in the bone defect sites were observed and photographed using a light microscope (Nikon Corporation).

Confocal microscopic analysis of Runx2

Effects of chitosan nanofiber scaffolds on expression of the transcription factor, Runx2, were analyzed using confocal microscopy as described previously.[37] After implantation of chitosan nanofiber scaffolds for 21 days, the animals were sacrificed, and their femurs were collected. After removing the muscle and connective tissues, the bone samples were fixed, embedded, and sliced. A mouse monoclonal antibody against Runx2 (Santa Cruz Biotechnology Inc., Dallas, TX, USA) was used in this study. Immunodetection of Runx2 in the femur was carried out at 4°C overnight. After washing, the slices were sequentially reacted with the secondary antibody and biotin-SP-conjugated AffiniPure anti-mouse immunoglobulin G (Jackson ImmunoResearch Laboratories, Inc., West Grove, PA, USA) at room temperature for 1 hour. After washing, the third antibody with Cy3-conjugated streptavidin (Jackson ImmunoResearch) was added to the femur slice and allowed to react at room temperature for 30 minutes. A confocal laser scanning microscope (Model FV500; Olympus Corporation, Tokyo, Japan) was utilized for sample observation. The excitation wavelength was set to 568 nm, while a 585 nm long-pass filter was used to collect the emitted light. Images were acquired and quantified using FLUOVIEW software (Olympus Corporation).

Immunohistological analyses of ALP and OCN

Effects of chitosan nanofiber scaffolds on levels of ALP and OCN in the bone defect sites were assayed using immunohistology as described previously.[36] After implantation of chitosan nanofiber scaffolds for 21 days, the animals were sacrificed. The femurs were removed, collected, and sliced into 5 μM sections. These femur specimen slices were fixed with a fixing reagent (acetone:methanol, 1:1) at −20°C for 10 minutes and incubated with 0.2% Triton X-100 at room temperature for 15 minutes. Immunodetection of ALP and OCN in bone tissues was carried out using polyclonal antibodies against rat ALP and OCN, respectively (Santa Cruz Biotechnology), by incubation at 4°C overnight. After washing, the slices were allowed to react with the secondary antibody at room temperature for 1 hour. Staining signals were visualized after reacting with 3,3′-diaminobenzidine. The specimen slices were observed and photographed using a light microscope (Nikon Corporation).

Immunoblotting analyses of ALP and OCN

After treatment, proteins were prepared from control and chitosan nanofiber-treated femurs in ice cold

radioimmunoprecipitation assay buffer (25 mM Tris-HCl [pH 7.2], 0.1% sodium dodecylsulfate [SDS], 1% Triton X-100, 1% sodium deoxycholate, 0.15 M NaCl, and 1 mM EDTA) as described previously.[36] To avoid protein degradation, a mixture of proteinase inhibitors, including 1 mM phenyl methyl sulfonyl fluoride, 1 mM sodium orthovanadate, and 5 mg/mL leupeptin, was added to the radioimmunoprecipitation assay buffer. Protein concentrations were quantified by a bicinchoninic acid protein assay kit (Pierce, Rockford, IL, USA). Cytosolic proteins (100 mg/well) were subjected to SDS-polyacrylamide gel electrophoresis (PAGE) and transferred to nitrocellulose membranes. These membranes were blocked with 5% non-fat milk at 37°C for 1 hour. ALP and OCN were immunodetected using related antibodies (Santa Cruz Biotechnology Inc.). β-Actin was detected using a mouse monoclonal antibody (Sigma-Aldrich) as the internal control. These protein bands were quantified using a digital imaging system (UVtec, Cambridge, UK).

Statistical analyses

The statistical significance of differences between the control and chitosan nanofiber-treated groups were evaluated using Student's *t*-test, and differences were considered statistically significant at *P*-values of <0.05. Statistical analyses between groups over time were carried out by a one-way analysis of variance.

Results

Preparation of chitosan nanofibers

To prepare uniform chitosan nanofibers, various concentrations of chitosan were fed and tested (Figure 2). In this assay, the other operational parameters were fixed at an applied voltage of 17 kV, a tip-to-collector distance of 12 cm, a flow rate of 0.2 mL/h, and an ambient temperature of 32°C. When the feeding concentration of chitosan was 50 mg/mL, undesirable beads formed (Figure 2A). In comparison, the appearance of beads decreased at 60 mg/mL (Figure 2B). At a concentration of 70 mg/mL, continuous chitosan nanofibers were obtained, and beaded structures were limited (Figure 2C). In contrast, when the concentration of chitosan was as high as 80 mg/mL, uniform chitosan nanofibers were generated with no beads or aggregations, and their average diameter was approximately 200 nm (Figure 2D).

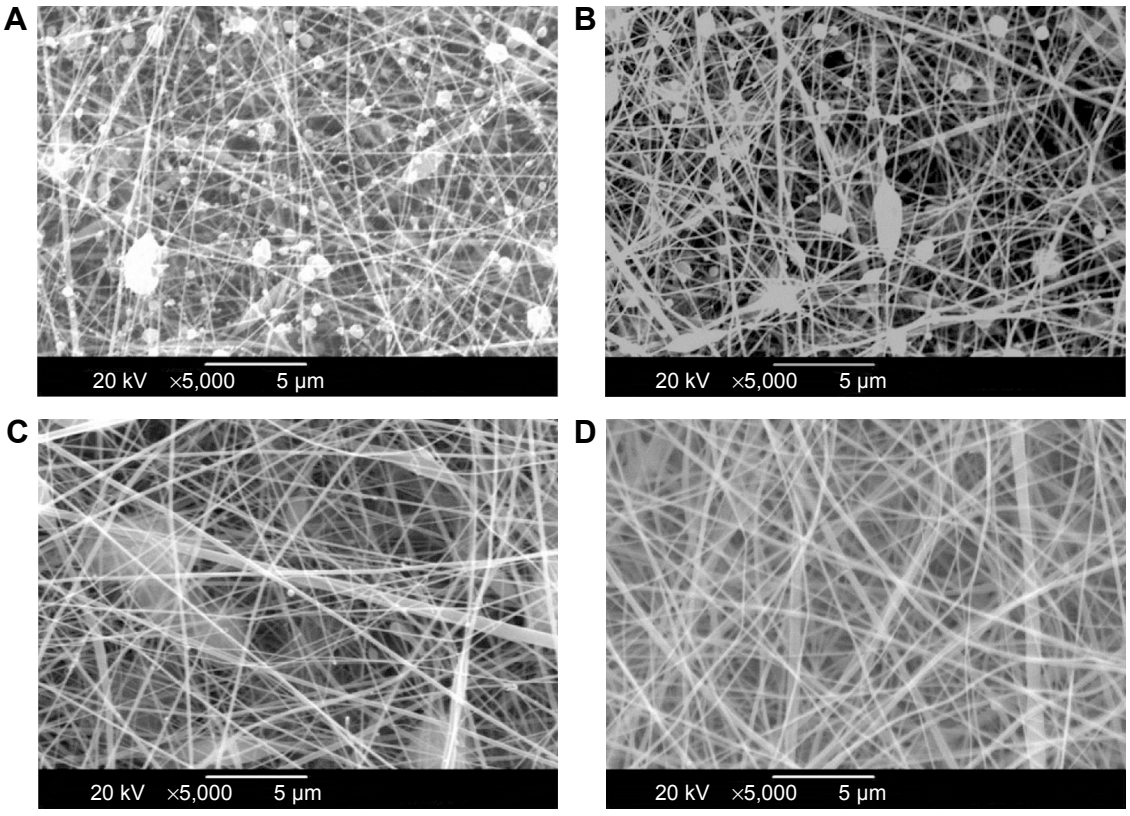

Figure 2 Preparation of electrospun chitosan nanofibers.
Notes: Chitosan at 50 mg/mL (**A**), 60 mg/mL (**B**), 70 mg/mL (**C**), and 80 mg/mL (**D**) was separately dissolved in the electrospinning solutions and electrospun into different chitosan nanofibers. The surface morphologies of these electrospun chitosan nanofibers were observed and photographed using scanning electron microscopy at 5,000×.

Administration of chitosan nanofiber scaffolds caused no hepatotoxicity or nephrotoxicity

Tissue toxicity of chitosan nanofiber scaffolds to the animals was evaluated using histological analyses (Figure 3). After implanting chitosan nanofiber scaffolds into bone defect sites of femurs for 21 days, results by the histological analyses showed that implantation of chitosan nanofiber scaffolds did not change hepatocyte morphologies or cell arrangements in the liver (Figure 3A). In parallel, implantation of chitosan nanofibers scaffolds into the bone defect sites did not cause nephrotoxicity (Figure 3B).

Implantation of chitosan nanofiber scaffolds improved bone healing

Effects of chitosan nanofiber scaffolds on bone repair were evaluated using μCT (Figure 4). Images of X-ray transmission revealed that bone fixing in the damaged site of the right femur spontaneously occurred within 21 days after surgery (Figure 4A, left panel). In comparison, implantation of chitosan nanofiber scaffolds increased the image densities, indicating better bone healing, in the bone defect site of the left femur (right panel). Supplementary analysis by μCT showed production of trabecular bone in the defect site of the right femur after implantation for 21 days (Figure 4B, left panel). Interestingly, compared with the control group, administration of chitosan nanofiber scaffolds into the defect site caused obvious enhancement of production of new trabecular bone (right panel).

Parameters tested and acquired by μCT analyses were quantified and statistically analyzed in order to further verify the effects of chitosan nanofibers on stimulation of bone healing (Figure 5). Implantation of chitosan nanofiber scaffolds into the defect site caused a significant 24% increase in trabecular bone numbers (Figure 5A). In addition, the trabecular bone thickness was meaningfully augmented by 22% following implantation of chitosan nanofiber scaffolds (Figure 5B). In contrast, after administering chitosan nanofiber scaffolds into the bone defect site for 21 days, the TPF was reduced by 19% (Figure 5C).

Bone histomorphometry was also carried out to demonstrate improved bone repair in insulted sites by chitosan

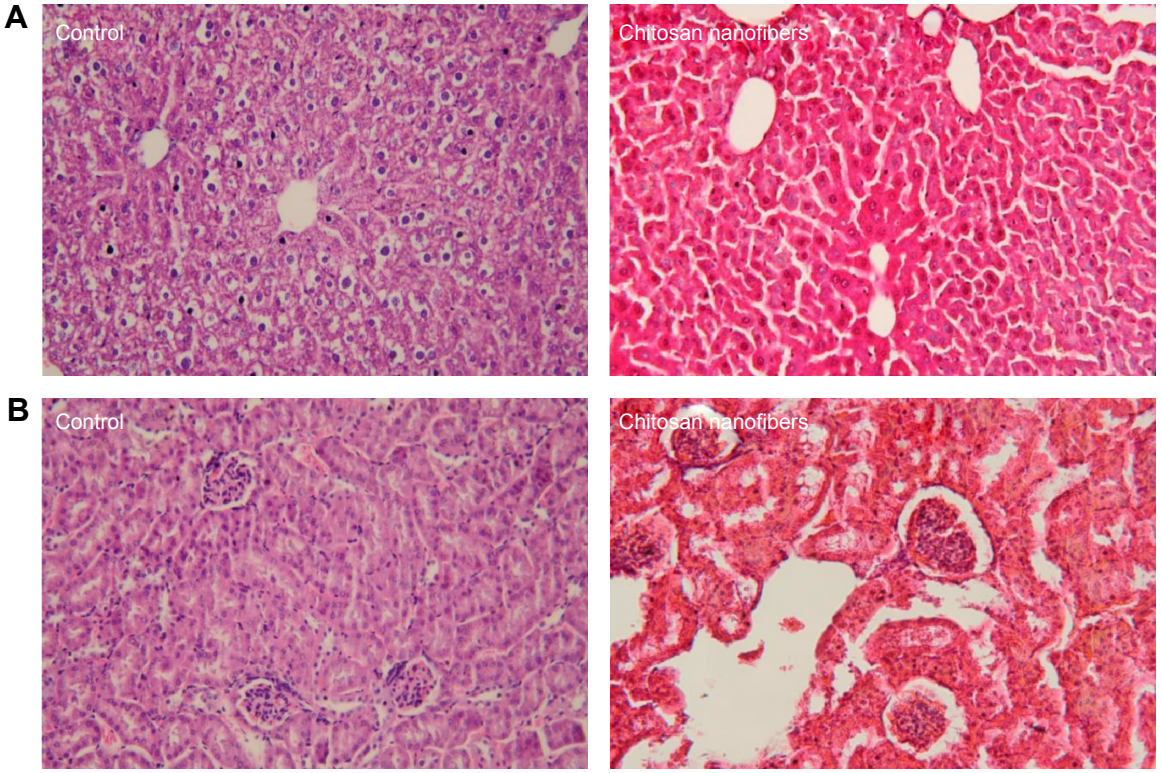

Figure 3 Toxicities of chitosan nanofibers to the liver and kidneys.
Notes: Bone defects were surgically created in the proximal femurs of male C57LB/L mice, and chitosan nanofibers were implanted into one defect for 21 days. After that period, animals were sacrificed, and the liver and kidneys were removed, cleaned, and weighed. These samples were fixed with paraformaldehyde and embedded in paraffin. Following slicing, liver (**A**) and kidney (**B**) specimens prepared from control (left panels) and chitosan nanofiber-treated (right panels) animals were stained with hematoxylin and eosin and observed and photographed under a light microscope at 200×. Only one defect was created in each proximal femur of an animal, and totally nine animals were treated in this study.

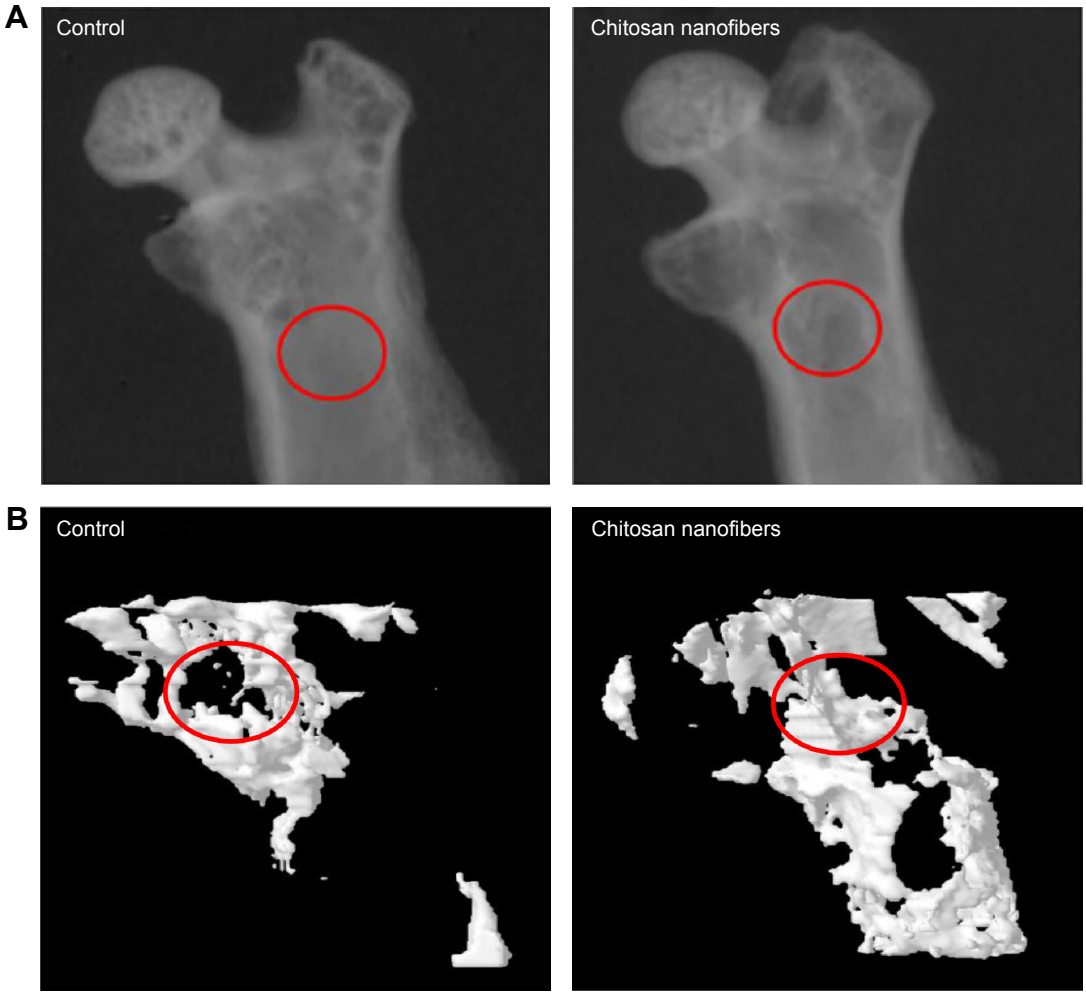

Figure 4 Effects of chitosan nanofiber scaffolds on trabecular bone production.
Notes: Bone defects were surgically created in the proximal femurs of male C57LB/L mice, and chitosan nanofibers were implanted into one defect for 21 days. After that period, animals were sacrificed, and the femurs were collected for analysis by μCT. The X-ray transmission images (**A**) and trabecular bone images (**B**) of the bone defects (red circles) in control and chitosan nanofiber scaffold-treated femurs are shown. Only one defect was created in each proximal femur of an animal, and totally nine animals were treated in this study.
Abbreviation: μCT, microcomputed tomography.

nanofiber scaffolds (Figure 6). Twenty-one days after creation of the bone defect, new trabecular bone had been produced and was observed in the defect site of the femurs (Figure 6, left panels). Nevertheless, implantation of chitosan nanofiber scaffolds into the defect site caused a remarkable increase in the manufacture of new trabecular bone compared with the control group (right panels).

Chitosan nanofiber scaffolds enhanced Runx2 expression

Roles of Runx2, a key transcription factor that controls osteoblast differentiation and maturation, in chitosan nanofiber scaffold-triggered improvement of bone healing were supplementary evaluated (Figure 7). Analysis by confocal microscopy revealed that Runx2 was detected in the bone defect site of the right femur (Figure 7A, left panel). Compared with the control group, implantation of chitosan nanofiber scaffolds into the damaged site of the left femur led to a significant enhancement in Runx2 expression (right panel). These fluorescent signals were quantified and statistically analyzed (Figure 7B). Administration of chitosan nanofiber scaffolds into the bone defect spot led to a 20-fold increase in levels of Runx2.

Chitosan nanofiber scaffolds stimulated syntheses of the bone biomarkers, ALP and OCN

To determine the mechanism of chitosan nanofiber-induced improvement in bone repair, the Runx2-mediated regulation of gene expressions of the bone biomarkers, ALP and

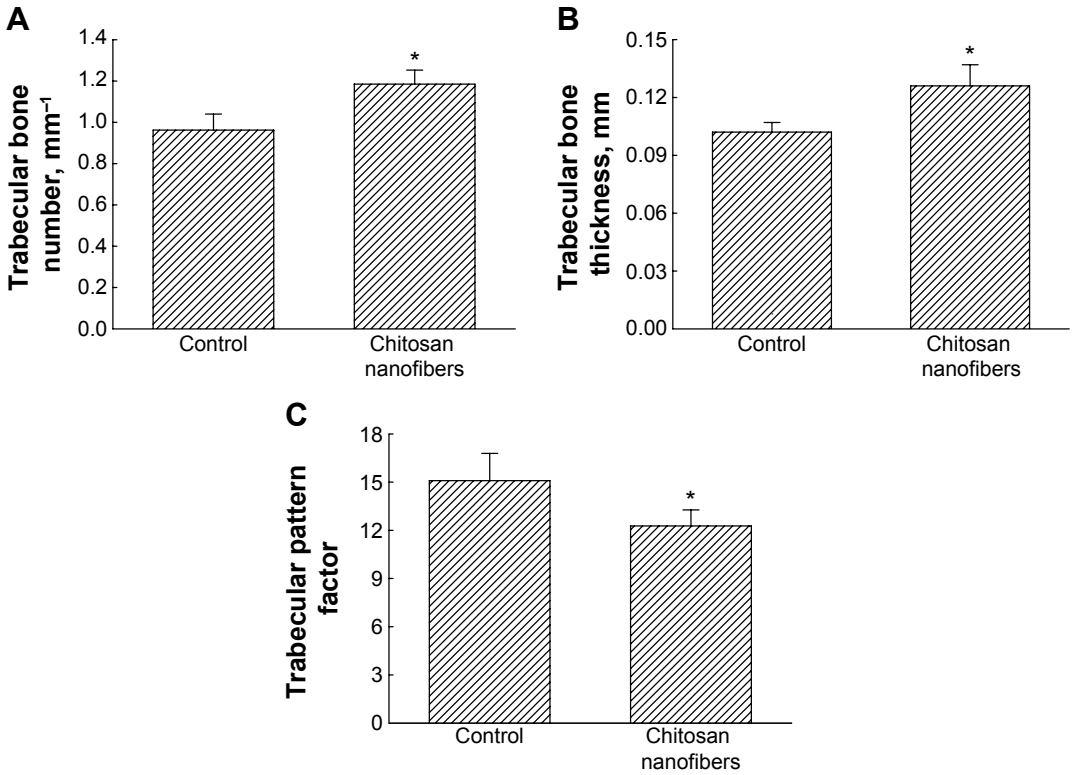

Figure 5 Improved effects of chitosan nanofiber scaffolds on bone healing.
Notes: Bone defects were surgically created in the proximal femurs of male C57LB/L mice, and chitosan nanofibers were implanted into one defect for 21 days. Only one defect was created in each proximal femur of an animal. After that period, animals were sacrificed, and the femurs were collected for analysis by μCT. The trabecular bone number (**A**), trabecular bone thickness (**B**), and trabecular parameter factor (**C**) were calculated and statistically analyzed. Each value represents the mean ± SEM for n=9. *Indicates that values significantly differed from the respective control, $P<0.05$.
Abbreviations: μCT, microcomputed tomography; SEM, standard error of mean.

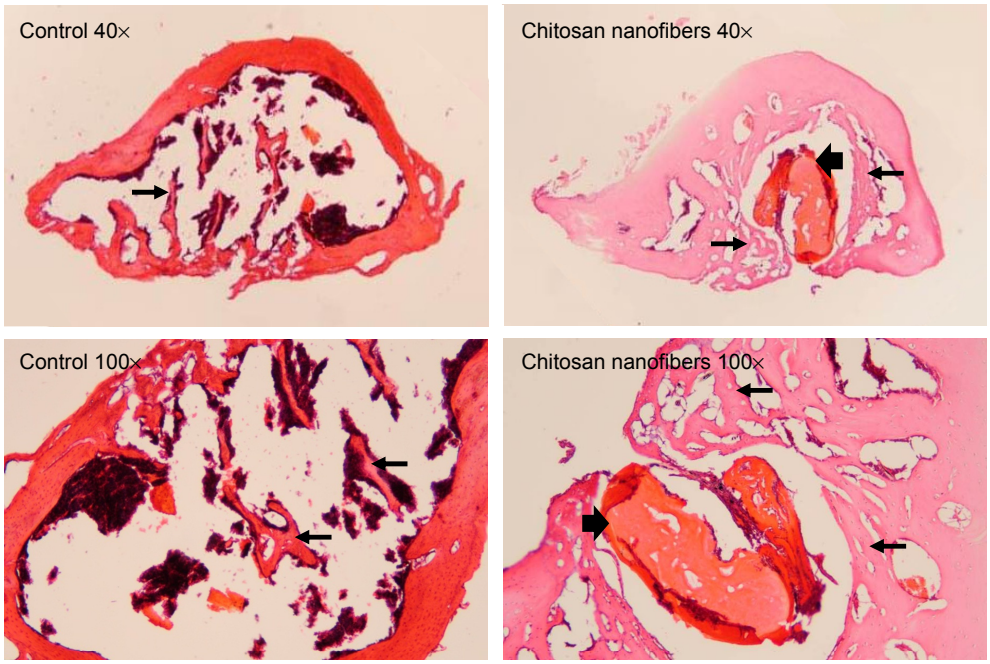

Figure 6 Effects of chitosan nanofiber scaffolds on bone healing using bone histomorphometry.
Notes: Bone defects were surgically created in the proximal femurs of male C57LB/L mice, and chitosan nanofibers were implanted into one defect for 21 days. After that period, animals were sacrificed, and the femurs were collected for a histological analysis. After removing the muscle and connective tissues, the femurs were decalcified, fixed, embedded in paraffin, and then sliced. These specimens were stained with hematoxylin and eosin. The stained signals were observed and photographed under a light microscope. Thin arrows indicate new bone areas, and thick arrows designate areas where the scaffolds were located. Only one defect was created in each proximal femur of an animal, and totally nine animals were treated in this study.

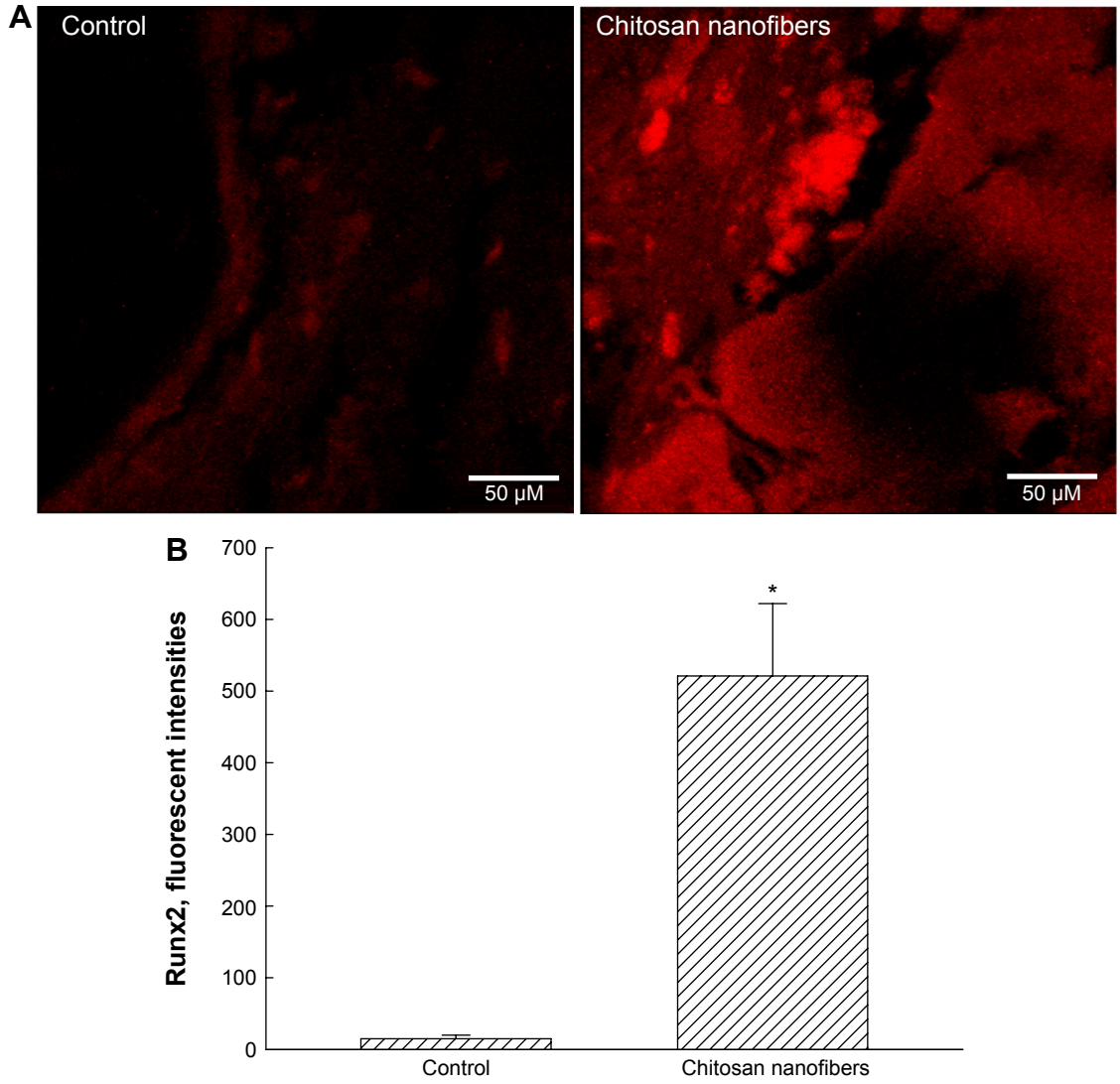

Figure 7 Effects of chitosan nanofiber scaffolds on levels of the transcriptional factor, Runx2, in bone defects.
Notes: Bone defects were created in the proximal femurs of male C57LB/L mice, and chitosan nanofibers were implanted into one defect for 21 days. Only one defect was created in each proximal femur of an animal. After that period, animals were sacrificed, and the femurs were collected for an immunohistological analysis of Runx2. After removing the muscle and connective tissues, the femurs were decalcified, fixed, embedded in paraffin, and then sliced. Levels of Runx2 were immunodetected by confocal microscopy (**A**). The fluorescent signals were quantified and statistically analyzed (**B**). Each value represents the mean ± SEM for n=9. *Indicates that values significantly differed from the respective control, $P<0.05$.
Abbreviations: Runx2, Runt-related transcription factor 2; SEM, standard error of mean.

OCN, were determined (Figure 8). Twenty-one days after creation of the bone defects, ALP was immunodetected in the damaged site of the right femurs (Figure 8A, left panel). In comparison, implantation of chitosan nanofiber scaffolds into the bone defect site of the left femur caused a detectable increase in levels of ALP (right panel). In parallel, OCN was immunodetected in the bone defect site of the right femur (Figure 8B, left panel). In contrast, implantation of chitosan nanofiber scaffolds into the bone defect site of the left femur caused a noteworthy elevation in amounts of OCN (right panel). In addition, administration of chitosan nanofiber scaffolds increased levels of ALP and OCN in the bone defect sites (Figure 8C, top two panels, lane 2). Amounts of β-actin were analyzed as the internal controls (bottom panel). These protein bands were quantified and statistically analyzed (Figure 8D). Implantation of chitosan nanofibers caused significant 151% and 79% increases in levels of ALP and OCN, respectively.

Discussion

This translational study shows the beneficial effects of chitosan nanofiber scaffolds on bone healing. In this study, we used a mouse model of bone defects to evaluate the effects of chitosan nanofibers on bone repair. The animal model of bone defects is a mutual and reliable prototype for assessing bone reconstruction and healing.[38] Implantation of chitosan

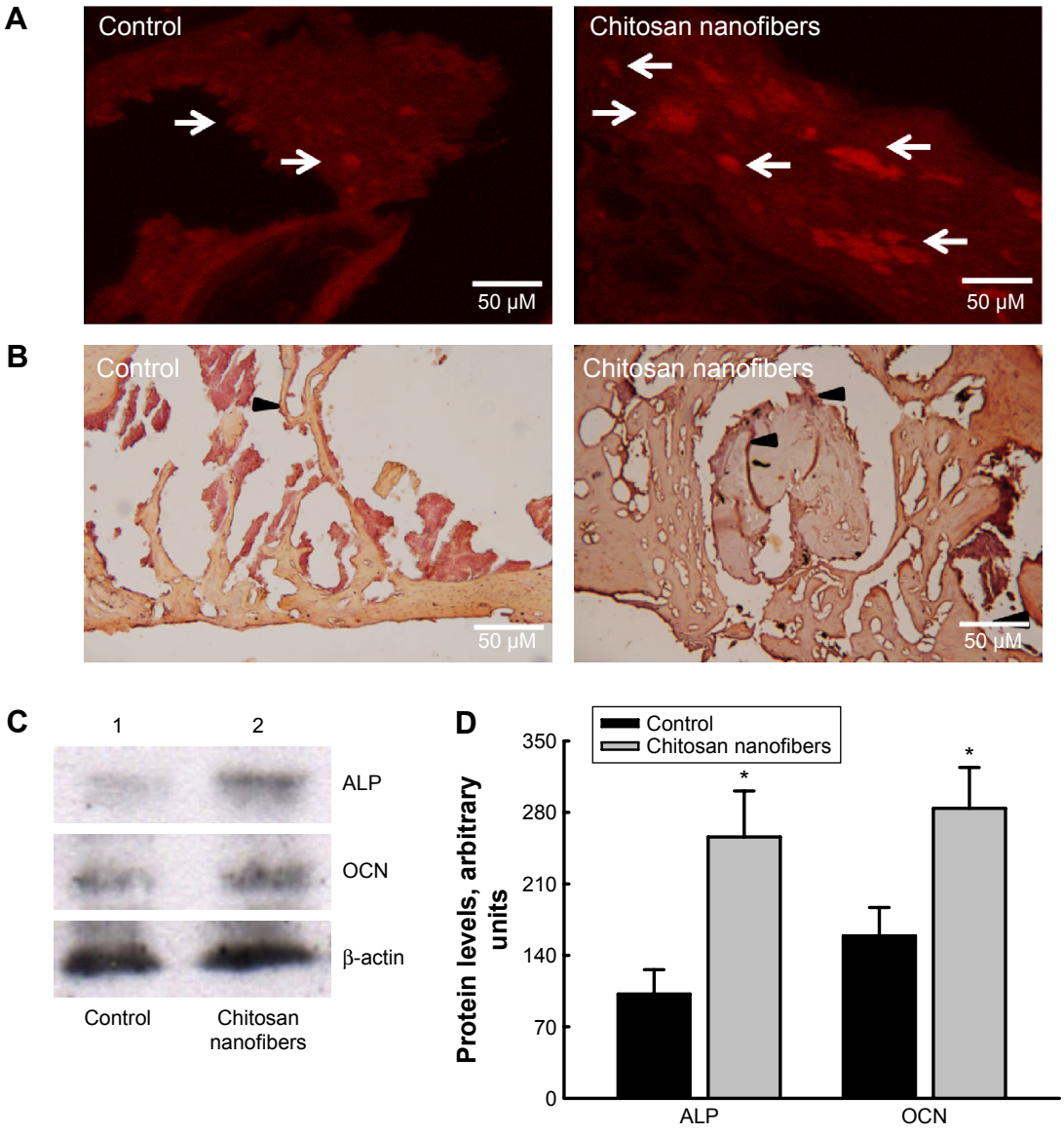

Figure 8 Effects of chitosan nanofibers on expressions of ALP and OCN in bone defects.
Notes: Bone defects were surgically created in the proximal femurs of male C57LB/L mice, and chitosan nanofiber scaffolds were implanted into one defect for 21 days. Only one defect was created in each proximal femur of an animal. After that period, animals were sacrificed, and the femurs were collected for immunohistological analyses of ALP (**A**) and OCN (**B**). Arrows/arrowheads indicate expressions of ALP and OCN. Proteins were prepared from control and chitosan nanofiber-treated femurs for immunoblotting analyses of ALP and OCN (**C**, top two panels). Amounts of β-actin were analyzed as the internal controls (bottom panel). These protein bands were quantified and statistically analyzed (**D**). Each value represents the mean ± SEM for n=6. *Indicates that values significantly differed from the respective control, $P<0.05$, 200×.
Abbreviations: ALP, alkaline phosphatase; OCN, osteocalcin; SEM, standard error of mean.

nanofiber scaffolds led to significant improvements in bone healing. Uusitalo et al reported that an increase in the production of new trabecular bone can reflect the status of bone remodeling and the process of bone healing.[32] This study showed augmentation of the production and thickness of new trabecular bone in the bone defect site. Thus, implantation of chitosan nanofiber scaffolds improved bone healing by raising the quantity and quality of trabecular bone. Also, this study demonstrated that implantation of chitosan nanofibers into mice did not cause hepatotoxicity or nephrotoxicity. Although chitosan is widely used for bone engineering, electrospun products of chitosan possess higher surface areas and porosity.[10,12,13,16] Moreover, our previous study showed that seeding osteoblasts onto chitosan nanofiber scaffolds can promote cell proliferation and maturation.[22] Therefore, our previous and present studies provide in vitro and in vivo data to verify the advantageous properties of chitosan nanofiber scaffolds on improving osteoblast activities and bone healing. Chitosan nanofibers can be comprised with other materials to emulate bone properties. For example, electrospun hydroxyapatite-containing chitosan nanofibers with compositional and structural features close to the natural

mineralized nanofibril counterparts can facilitate differentiation and maturation of osteoblasts.[39,40] Zhang et al reported that electrospun hydroxyapatite/collagen/chitosan composite worked as a highly biomimetic and bioactive nanofibrous structure and could stimulate osteoregeneration.[41] Recently, Sambudi et al reported a more suitable environment provided by the chitosan/poly(vinyl alcohol) reinforced with $CaCO_3$ for cell growth than the chitosan/poly(vinyl alcohol) and the chitosan/poly(vinyl alcohol) reinforced with apatite.[42] In comparison, the present study used an animal model to demonstrate the beneficial effects of chitosan nanofibers on improvement of bone healing. Bone fractures are a common accident of modern people. Moreover, osteoporosis-associated bone fractures are a major risk factor for disability and even death of patients with osteoporosis.[4] Nonetheless, no effective drug has been developed for treating bone fractures so far. The present results indicate the potential of chitosan nanofiber scaffolds for therapy of bone defects and fractures.

We efficaciously created uniform electrospun nanofibers of chitosan. The applicable ranges and optimization of operational parameters were initially tested for electrospinning of chitosan (Table 1). The entanglement force was dominated by chitosan concentrations and temperatures, while the strength of the electrostatic force was related to applied voltages, discharge distances, and feeding rates. By applying these parameters in appropriate ranges, continuous nanofibers were produced. In this study, we fabricated uniform chitosan nanofibers with highly consistent and nanoscale diameters, limited beads, and very little agglomeration when the optimized conditions were used, which was achieved by an equilibrium between repulsion Columbic forces and entanglement forces. Although the electrospinning of pure chitosan was carried out in a few previous studies,[43,44] this was the first research to systematically optimize all of the operational parameters for the electrospinning of chitosan using TFA/DCM as the co-solvents. Our results indicate that a concentrated chitosan solution was beneficial for fabricating continuous and uniform nanofibers, which was in agreement with previous findings from the electrospinning of poly(lactic acid) and poly(ethylene oxide).[45,46] In addition, previous studies reported that there was a lower limit of chitosan concentrations for forming nanofibers because a low chitosan concentration was insufficient to provide intramolecular entanglement forces to maintain a continuous electrospinning jet.[43,44] The entanglement force increased with the polymer concentration that prevented the thinning process in the formation of nanofibers by resisting the repulsion Columbic forces in electrospinning.[45] In other words, a balance between viscous and electrostatic forces is necessary to produce uniform electrospun chitosan nanofibers.

Chitosan nanofibers can trigger the production of new trabecular bone and then improve bone healing. Trabecular bone is one of two typical osseous tissues that are involved in bone formation.[47] Analysis by μCT showed that after implantation of chitosan nanofiber scaffolds, the trabecular bone numbers were significantly higher. A similar result was confirmed by a bone histomorphometric assessment. An increase in the production of new trabecular bone implies enhancement of metabolic rates in the bone microenvironment, reflecting the status of bone healing.[32] Furthermore, our results showed that chitosan nanofibers augmented the thickness of trabecular bone. Thicker trabecular bone indicates a better mechanic load distribution, which is helpful for bone recovery.[48] Administration of chitosan nanofiber scaffolds to mice suffering from a bone defect caused a significant reduction in the TPF value. TPF is a histomorphometric parameter that simply quantifies the bone microarchitecture.[49] A decrease in the TPF value characterizes stronger trabecular connectivity.[35] Our present results from imaging, parameter, and histomorphometric analyses showed that implantation of chitosan nanofiber scaffolds enhanced the production, thickness, and connectivity of trabecular bone. Consequently, chitosan nanofibers can improve the processing of bone remodeling and fixing. Runx2 contributes to chitosan nanofiber-induced development of bone repair. Implantation of chitosan nanofiber scaffolds into the bone defect site led to substantial enhancement of Runx2 expression compared with the control group. Osteogenesis is a crucial stage in bone formation and remodeling.[7] Throughout osteogenic differentiation, Runx2 gene expression can be regulated by bone morphogenetic proteins.[50] Previous studies proposed that chitosan nanofibers may induce Runx2 gene expression in osteoblasts via the bone morphogenetic protein signaling pathway.[22,51] Proliferation, differentiation, and maturation of osteoblasts are positively related to the rate of osteogenesis.[8] Multiple genes are involved in regulating osteoblast activities and osteogenesis.[4,6] Runx2 is an indispensable transcription factor for regulating these osteogenesis-related gene expressions.[26] A previous study reported that loading stress-induced upregulation of Runx2 in the rat ulna was closely associated with improvements in fracture healing.[27] Under inflammation, levels of Runx2 in osteoblasts were augmented, induced antiapoptotic *Bcl-2* gene expression, and protected cells against apoptotic insults.[31] In our previous study, we also showed that chitosan nanofiber scaffolds could trigger osteoblast proliferation and maturation through a Runx2-dependent pathway.[22] Therefore,

implantation of chitosan nanofiber scaffolds into the bone defect site effectively improved bone healing through Runx2-mediated regulation of certain osteogenesis-related gene expressions.

Chitosan nanofibers can induce ALP and OCN expressions and then improve bone repair. Following implantation of chitosan nanofiber scaffolds, levels of ALP in the defect site increased. ALP, a typical bone marker, functionally participates in regulating osteoblast activities.[28] Augmentation of ALP correspondingly specifies growth in osteoblast proliferation and maturation. The present results confirm our previous findings that chitosan nanofibers can induce osteoblast growth and mineralization.[22] In addition, amounts of OCN in the bone defect site were concurrently enhanced following treatment with chitosan nanofiber scaffolds. OCN is an early osteoblast marker that controls osteoblast differentiation and bone ECM mineralization.[29] Runx2 was also demonstrated to transcriptionally regulate OCN and ALP gene expressions.[52] A previous study further showed that Runx2 stimulated differentiation of multipotential mesenchymal ROB-C26 cells into mature osteoblasts via regulating OCN and ALP gene expressions.[30] Hence, chitosan nanofiber scaffolds may induce OCN and ALP expressions through upregulating Runx2 levels in bone-insult sites. ECM mineralization and osteoblast maturation are two final stages in the process of osteogenesis.[8,49] Our previous study proved the beneficial action of chitosan nanofiber scaffolds on osteoblast mineralization.[22] Therefore, our results propose that implantation of chitosan nanofiber scaffolds induces Runx2-mediated ALP and OCN expressions and then stimulates osteogenesis and bone healing.

Conclusion

In summary, we successfully produced uniform chitosan nanofiber scaffolds at the nanoscale. This study separately created an animal model of bone defects to examine effects of chitosan nanofiber scaffolds on bone healing. Our results present the beneficial properties of chitosan nanofiber scaffolds on improving bone remodeling and fixation. Analyses by μCT further demonstrated that implantation of chitosan nanofiber scaffolds caused significant augmentation in the number and thickness of trabecular bone and a reduction in TPF values. In addition, bone histomorphometric assessments also showed improved effects of chitosan nanofiber scaffolds on the production of new trabecular bone. As to the mechanism, analysis by confocal microscopy revealed that implantation of chitosan nanofiber scaffolds significantly augmented levels of Runx2 in the defect site. Sequentially, amounts of OCN and ALP in the bone damaged site were raised following implantation of chitosan nanofiber scaffolds. Therefore, this study shows beneficial effects of chitosan nanofiber scaffolds on stimulating bone healing through enhancing the production, thickness, and connectivity of trabecular bone. The molecular mechanisms of chitosan nanofiber-induced improvement of bone repair may be via Runx2-mediated regulation of ALP and OCN gene expressions. Our present results designate the clinical potential of chitosan nanofiber scaffolds for therapy of bone diseases such as bone defects, as well as common and osteoporosis-related bone fractures.

Acknowledgments

This study was supported by Taipei Medical University and National Taiwan University of Science and Technology (TMU-NTUST-101-01), Wan-Fang Hospital (104swf04), and the Ministry of Science and Technology (MOST 104-2314-B-038-004-MY3), Taipei, Taiwan. We thank the Taiwan Mouse Clinic (MOST 104-2325-B-001-011) which is funded by the National Research Program for Biopharmaceuticals at the Ministry of Science and Technology of Taiwan for technical support in micro-computed tomographic experiment.

Disclosure

The authors report no conflicts of interest in this work.

References

1. Seeman E, Delmas PD. Bone quality – the material and structural basis of bone strength and fragility. *N Engl J Med*. 2006;354:2250–2261.
2. Karsdal MA, Martin TJ, Henriksen K. Osteoclast-derived coupling factors in bone remodeling. *Calcif Tissue Int*. 2014;94:88–97.
3. Rachner TD, Khosla S, Hofbauer LC. Osteoporosis: now and the future. *Lancet*. 2011;377:1276–1287.
4. Cauley JA, Chalhoub D, Kassem AM, Fuleihan Gel-H. Geographic and ethnic disparities in osteoporotic fractures. *Nat Rev Endocrinol*. 2014;10:338–351.
5. Geris L, Gerisch A, Sloten JV, Weiner R, Oosterwyck HV. Angiogenesis in bone fracture healing: a bioregulatory model. *J Theor Biol*. 2008;251:137–158.
6. Shapiro F. Bone development and its relation to fracture repair. The role of mesenchymal osteoblasts and surface osteoblasts. *Eur Cells Mater*. 2008;15:53–76.
7. Aubin JE, Liu F, Malaval L, Gupta AK. Osteoblast and chondroblast differentiation. *Bone*. 1995;17:77S–83S.
8. Giustina A, Mazziotti G, Canalis E. Growth hormone, insulin-like growth factors, and the skeleton. *Endocr Rev*. 2008;29:535–559.
9. Tan ML, Shao P, Friedhuber AM, et al. The potential role of free chitosan in bone trauma and bone cancer management. *Biomaterials*. 2014;35:7828–7838.
10. Suh JK, Matthew HW. Application of chitosan-based polysaccharide biomaterials in cartilage tissue engineering: a review. *Biomaterials*. 2000;21:2589–2598.
11. Ueno H, Mori T, Fujinaga T. Topical formulations and wound healing applications of chitosan. *Adv Drug Deliv Rev*. 2001;52:105–115.
12. Costa-Pinto AR, Reis RL, Neves NM. Scaffolds based bone tissue engineering: the role of chitosan. *Tissue Eng Part B*. 2011;17:331–347.

13. Di Martino A, Sittinger M, Risbud MV. Chitosan: a versatile biopolymer for orthopaedic tissue-engineering. *Biomaterials*. 2005;26:5983–5990.
14. Koc A, Finkenzeller G, Elcin AE, Stark GB, Elcin YM. Evaluation of adenoviral vascular endothelial growth factor-activated chitosan/hydroxyapatite scaffold for engineering vascularized bone tissue using human osteoblasts: in vitro and in vivo studies. *J Biomater Appl*. 2014;29:748–760.
15. Fernandez T, Olave G, Valencia CH, et al. Effects of calcium phosphate/chitosan composite on bone healing in rats: calcium phosphate induces osteon formation. *Tissue Eng Part A*. 2014;20:1948–1960.
16. Jayakumar R, Prabaharan M, Nair SV, Tamura H. Novel chitin and chitosan nanofibers in biomedical applications. *Biotechnol Adv*. 2010;28:142–150.
17. Wang W, Itoh S, Konno K, et al. Effects of Schwann cell alignment along the oriented electrospun chitosan nanofibers on nerve regeneration. *J Biomed Mater Res A*. 2009;91:994–1005.
18. Chen ZG, Wang PW, Wei B, Mo XM, Cui FZ. Electrospun collagen-chitosan nanofiber: a biomimetic extracellular matrix for endothelial cell and smooth muscle cell. *Acta Biomate*. 2010;6:372–382.
19. Jancár J, Slovíková A, Amler E, et al. Mechanical response of porous scaffolds for cartilage engineering. *Physiol Res*. 2007;56:S17–S25.
20. Liu H, Peng H, Wu Y, et al. The promotion of bone regeneration by nanofibrous hydroxyapatite/chitosan scaffolds by effects on integrin-BMP/Smad signaling pathway in BMSCs. *Biomaterials*. 2013;34:4404–4417.
21. Shin SY, Park HN, Kim KH, et al. Biological evaluation of chitosan nanofiber membrane for guided bone regeneration. *J Periodontol*. 2005;76(10):1778–1784.
22. Ho MH, Liao MH, Lin YL, Lai CH, Lin PI, Chen RM. Improving effects of chitosan nanofiber scaffolds on osteoblast proliferation and maturation. *Int J Nanomed*. 2004;9:4293–4304.
23. Stein GS, Lian JB, Stein JL, Van Wijnen AJ, Montecino M. Transcriptional control of osteoblast growth and differentiation. *Physiol Rev*. 1996;76:593–624.
24. Vandenput L, Ohlsson C. Estrogens as regulators of bone health in men. *Nat Rev Endocrinol*. 2009;5:437–443.
25. Hawse JR, Subramaniam M, Ingle JN, Oursler MJ, Rajamannan NM, Spelsberg TC. Estrogen-TGF-β cross-talk in bone and other cell types: role of TIEG, Runx2, and other transcription factors. *J Cell Biochem*. 2008;103:383–392.
26. Komori T. Signaling networks in RUNX2-dependent bone development. *J Cell Biochem*. 2011;112:750–755.
27. Wohl GR, Towler DA, Silva MJ. Stress fracture healing: fatigue loading of the rat ulna induces upregulation in expression of osteogenic and angiogenic genes that mimic the intramembranous portion of fracture repair. *Bone*. 2009;44:320–330.
28. Zhou H, Choong P, McCarthy R, Chou ST, Martin TJ, Ng KW. In situ hybridization to show sequential expression of osteoblast gene markers during bone formation in vivo. *J Bone Miner Res*. 1994;9:1489–1499.
29. van Leeuwen JP, van Driel M, van den Bemd GJ, Pols HA. Vitamin D control of osteoblast function and bone extracellular matrix mineralization. *Crit Rev Eukaryot Gene Expr*. 2001;11:199–226.
30. Takahashi T, Kato S, Suzuki N, Kawabata N, Takagi M. Autoregulatory mechanism of Runx2 through the expression of transcription factors and bone matrix proteins in multipotential mesenchymal cell line, ROB-C26. *J Oral Sci*. 2005;47:199–207.
31. Ho WP, Chan WP, Hsieh MS, Chen RM. Runx2-mediated *Bcl-2* gene expression contributes to nitric oxide protection against oxidative stress-induced osteoblast apoptosis. *J Cell Biochem*. 2009;108:1084–1093.
32. Uusitalo H, Rantakokko J, Ahonen M, et al. A metaphyseal defect model of the femur for studies of murine bone healing. *Bone*. 2001;28:423–429.
33. Chang HC, Tai YT, Cherng YG, et al. Resveratrol attenuates high-fat diet-induced disruption of the blood-brain barrier and protects brain neurons from apoptotic insults. *J Agric Food Chem*. 2014;62:3466–3475.
34. Seul KJ, Cho HS, Heo SH, et al. Osteoblast-specific expression of MEF induces osteopenia through downregulation of osteoblastogenesis and upregulation of osteoclastogenesis. *J Bone Miner Res*. 2011;26:341–350.
35. Toben D, Schroeder I, El Khassawna T, et al. Fracture healing is accelerated in the absence of the adaptive immune system. *J Bone Miner Res*. 2011;26:113–124.
36. Lee YE, Liu HC, Lin YL, et al. *Drynaria fortunei* J. Sm. improves the bone mass of ovariectomized rats through osteocalcin-involved endochondral ossification. *J Ethnopharmacol*. 2014;158(pt A):98–104.
37. Lin JW, Chen JT, Hong CY, et al. Honokiol traverses the blood-brain barrier and induces apoptosis of neuroblastoma cells via an intrinsic Bax-mitochondrion-cytochrome c-caspase protease pathway. *Neuro Oncol*. 2012;14:302–314.
38. Zhu W, Wang D, Peng L, et al. An experimental study on the application of radionuclide imaging in repairing bone defects. *Artif Cells Nanomed Biotechnol*. 2013;41:304–308.
39. Zhang Y, Venugopal JR, El-Turki A, Ramakrishna S, Su B, Lim CT. Electrospun biomimetic nanocomposite nanofibers of hydroxyapatite/chitosan for bone tissue engineering. *Biomaterials*. 2008;29:4314–4322.
40. Frohbergh ME, Katsman A, Botta GP, et al. Electrospun hydroxyapatite-containing chitosan nanofibers crosslinked with genipin for bone tissue engineering. *Biomaterials*. 2012;33:9167–9178.
41. Zhang Y, Reddy VJ, Wong SY, et al. Enhanced biomineralization in osteoblasts on a novel electrospun biocomposite nanofibrous substrate of hydroxyapatite/collagen/chitosan. *Tissue Eng Part A*. 2010;16:1949–1960.
42. Sambudi NS, Sathyamurthy M, Lee GM, Park SB. Electrospun chitosan/poly(vinyl alcohol) reinforced with CaCO3 nanoparticles with enhanced mechanical properties and biocompatibility for cartilage tissue engineering. *Compos Sci Technol*. 2015;106:76–84.
43. Ohkawa K, Cha D, Kim H, Nishida A, Yamamoto H. Electrospinning of chitosan. *Macromol Rapid Commun*. 2004;25:1600–1605.
44. Torres-Giner S, Ocio MJ, Lagaron JM. Development of active antimicrobial fiber based chitosan polysaccharide nanostructures using electrospinning. *Eng Life Sci*. 2008;8:303–314.
45. Deitzel JM, Kleinmeyer J, Harris D, Tan NCB. The effect of processing variables on the morphology of electrospun nanofibers and textiles. *Polymer*. 2001;42:261–272.
46. Chen JW, Tseng KF, Delimartin S, Lee CK, Ho MH. Preparation of biocompatible membranes by electrospinning. *Desalination*. 2008;233:48–54.
47. Wongdee K, Krishnamra N, Charoenphandhu N. Endochondral bone growth, bone calcium accretion, and bone mineral density: how are they related? *J Physiol Sci*. 2012;62:299–307.
48. Wang H, Ji B, Liu XS, Guo XE, Huang Y, Hwang KC. Analysis of microstructural and mechanical alterations of trabecular bone in a simulated three-dimensional remodeling process. *J Biomech*. 2012;45:2417–2425.
49. Hahn M, Vogel M, Pompesius-Kempa M, Delling G. Trabecular bone pattern factor – a new parameter for simple quantification of bone microarchitecture. *Bone*. 1992;13:327–330.
50. Trzeciakiewicz A, Habauzit V, Mercier S, et al. Hesperetin stimulates differentiation of primary rat osteoblasts involving the BMP signalling pathway. *J Nutr Biochem*. 2010;21:424–431.
51. Huang TY, Chen TL, Liao MH, et al. *Drynaria fortunei* J. Sm. promotes osteoblast maturation by inducing differentiation-related gene expression and protecting against oxidative stress-induced apoptotic insults. *J Ethnopharmacol*. 2010;131:70–77.
52. Wang H, Huo N, Li F, et al. Osteogenic role of endosomal chloride channels in MC3T3-E1 cells. *Mol Cell Biochem*. 2010;342:191–199.